

Review

# A Survey of Supramolecular Aggregation Based on Main Group Element···Selenium Secondary Bonding Interactions—A Survey of the Crystallographic Literature

Edward R. T. Tiekink 

Research Centre for Crystalline Materials, School of Science and Technology, Sunway University, 47500 Bandar Sunway, Selangor Darul Ehsan, Malaysia; edwardt@sunway.edu.my; Tel.: +60-3-7491-7181

Received: 30 May 2020; Accepted: 10 June 2020; Published: 12 June 2020



**Abstract:** The results of a survey of the crystal structures of main group element compounds (M = tin, lead, arsenic, antimony, bismuth, and tellurium) for intermolecular M···Se secondary bonding interactions is presented. The identified M···Se interactions in 58 crystals can operate independent of conventional supramolecular synthons and can sustain zero-, one-, two, and, rarely, three-dimensional supramolecular architectures, which are shown to adopt a wide variety of topologies. The most popular architecture found in the crystals stabilized by M···Se interactions are one-dimensional chains, found in 50% of the structures, followed by zero-dimensional (38%). In the majority of structures, the metal center forms a single M···Se contact; however, examples having up to three M···Se contacts are evident. Up to about 25% of lead(II)-/selenium-containing crystals exhibit Pb···Se tetrel bonding, a percentage falling off to about 15% in bismuth analogs (that is, pnictogen bonding) and 10% or lower for the other cited elements.

**Keywords:** secondary bonding; supramolecular; crystal engineering; tetrel bonding; pnictogen bonding; chalcogen bonding; selenium; structural chemistry; main group elements

## 1. Introduction

The term “chalcogen bonding” has only relatively recently been incorporated in the crystallography lexicon [1] and refers to a non-covalent interaction featuring a Group VI element, for example and relevant to the present bibliographic survey, selenium, functioning as an electrophilic center [2–4]. The current use of the term “chalcogen bonding” notwithstanding, such interactions have long been recognized in the chemical crystallography community [5–7] but under the guise of “secondary bonding” [7]. Secondary bonding encompasses a range of bonding circumstances such as classic Lewis acid/Lewis base interactions occurring between a metal center, such as a main group element (or p-block element), acting as the acid, and a lone-pair of electrons residing on the Lewis base. The non-covalent binding between atoms under these circumstances, being electrostatic in nature, is in keeping with expectation, that is, opposites attract. More perplexing are those contacts occurring between two ostensibly electron-rich species such a low-valent main group element, that is, having a lone-pair of electrons interacting with an electron-rich element such as selenium. In the structural chemistry of selenium, a very early example of the discussion of the latter type of interaction, that is, an intermolecular Se···O contact between electron-rich species, and the description of the supramolecular assembly stabilized by this interaction, was reported in 1972 [8], and is now classified as a chalcogen bond. The rationale for the formation of chalcogen bonds and indeed,

for example, allied tetrel, pnictogen and halogen bonding interactions in which a Group XIV, XV, and XVII element, respectively, functions as the electrophilic center, revolves around the concept of a polar cap or  $\sigma$ -hole [9–14]. Very briefly, a  $\sigma$ -hole refers to an electron-deficient region at the extension of a covalent bond or at the tip of a lone-pair of electrons, which is available, being a pseudo Lewis acidic site, for interaction with an electron-rich region, such as a lone-pair of electrons, of a participating species. Examples of both types of interaction scenarios between a main group element and selenium are found herein and, therefore, the generic term “secondary bonding” is employed throughout. However, the purpose of this present review of the relevant structural data is not to evaluate bonding considerations, rather to highlight the prevalence of  $M \cdots Se$  secondary bonding and the supramolecular architectures they sustain. The present literature survey was conducted in continuation of a long-held interest in secondary bonding and the supramolecular patterns stabilized by these interactions [15–23], and is aimed at summarizing all of the known  $M \cdots Se$  supramolecular contacts operating in the crystals of main group element species with  $M =$  tin, lead, arsenic, antimony, bismuth, and tellurium, and to provide comprehensive descriptions of the supramolecular aggregates arising from these in a consistent fashion.

## 2. Methods

In the present analysis of the crystallographic literature, the Cambridge Structural Database (CSD; version 5.41) [24] was searched employing ConQuest (version 2.0.4) [25] for  $M \cdots Se$  contacts in crystals based on a distance criterion, that is, the separation between the respective main group element ( $M =$  tin, lead, arsenic, antimony, bismuth, and tellurium) and selenium had to be equal to or less than the sum of the respective van der Waals radii being 1.90 Å for selenium, 2.17 and 2.02 Å for tin and lead, 1.85, 2.00, 2.00 for arsenic, antimony, and bismuth, and 2.06 Å for tellurium [25]. In addition, general criteria were applied; structures with  $R > 0.100$  were excluded along with disordered structures and polymeric species. All retrieved structures were manually evaluated to ensure that the putative  $M \cdots Se$  interaction was operating independently of other supramolecular synthons, such as conventional hydrogen bonding. All crystallographic diagrams are original, being generated with DIAMOND [26].

## 3. Results

The following gives an outline of the supramolecular association formed between selenium and, in turn, the main group elements,  $M =$  tin, lead, arsenic, antimony, bismuth, and tellurium, as revealed by X-ray crystallography. Traditionally, when searching for structures with secondary bonding interactions [7], such as  $A-D \cdots M$  in the present analysis where  $D = Se$ , contacts between the two elements occurring at distances longer than the assumed sum of the covalent radii but, less than the sum of the van der Waals radii are identified. In this scenario, the angle at the selenium atom might be expected to be close to  $180^\circ$ . However, this is an oversimplification for two key reasons. Firstly, if the donor is selenium(II), as in the majority of the structures described herein, there are two lone-pairs of electrons available for binding to  $M$ ; for selenium(IV), there is one lone-pair. In addition, the selenium atom may be bound to two or more other atoms; for example, the interaction might be of the type  $A_2Se \cdots M$ ,  $A_3Se \cdots M$ , and so on. In these ways, the  $A-D \cdots M$  contact is distinct from a conventional hydrogen bonding interaction or an analogous halogen bonding interaction. In instances where the selenium-bound lone-pair of electrons is assumed to interact with the  $\sigma$ -hole of the main group element-bound lone-pair of electrons, as appears to be the case in most of the examples discussed in 3.1–3.6, the lone-pair may not necessarily be diagonally opposite to a covalent bond. It is for these reasons, that is, the influence of the bonding circumstances and the variable coordination geometries of the donor and acceptor atoms, angular information is not included in the descriptions of the structures. The identified  $M \cdots Se$  contacts occur independently of other obvious supramolecular association such as hydrogen bonding interactions. The supramolecular

aggregation patterns are discussed in the order zero-, one-, two-, and three-dimensional. Within each category, mononuclear species are described before binuclear species, etc.

### 3.1. Tin Compounds Featuring Sn···Se Interactions in their Crystals

There are 13 compounds featuring Sn···Se secondary bonding interactions in their crystals, **1–13**, and the chemical structures for these are shown in Figure 1. The aggregation patterns involve both tin(II) and tin(IV) centers and encompass zero-, one- and, two, and three-dimensional architectures.

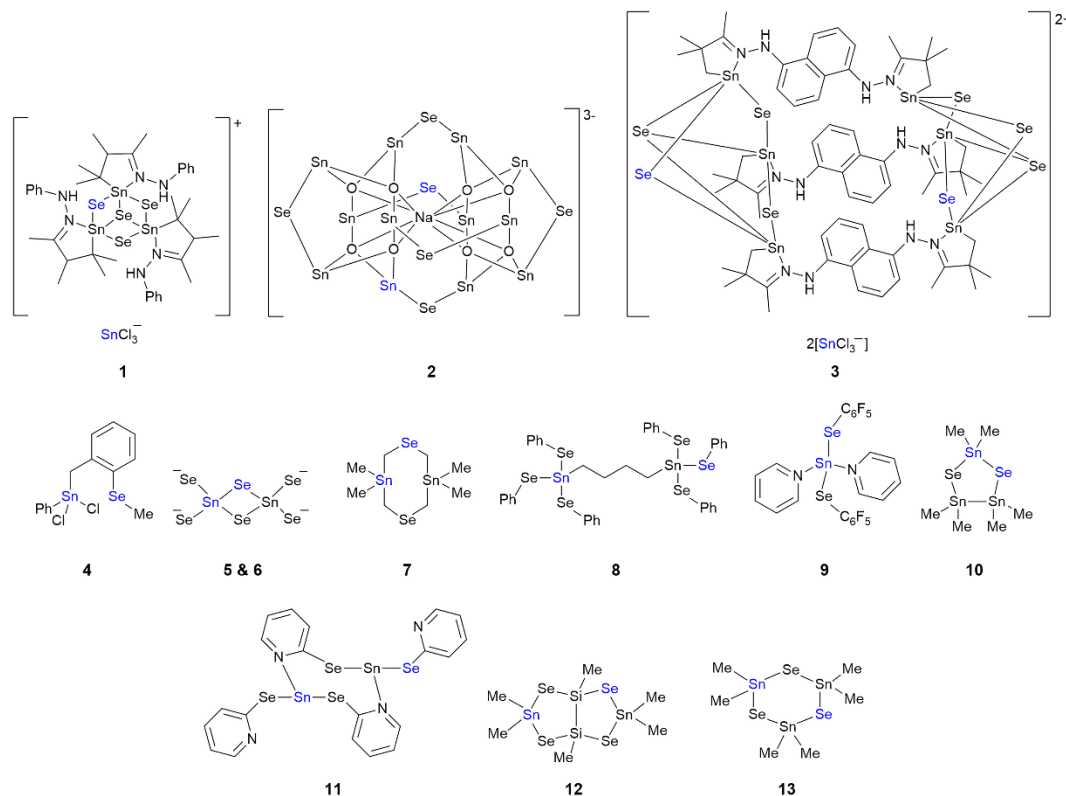


**Figure 1.** Chemical diagrams for tin compounds **1–13**. The atoms participating in the Sn···Se interactions are highlighted in blue.

The first three structures to be discussed have rather complicated compositions, but the supramolecular association between the interacting species is relatively simple, leading to zero-dimensional aggregates in each case. In **1** [27], comprising interacting cations and anions, the former contains a central Sn<sub>3</sub>Se<sub>3</sub> core capped by a μ<sub>3</sub>-Se atom forming bonds to the each of the three tin atoms of the core, and the counter-anion is [SnCl<sub>3</sub>]<sup>−</sup>. The tin(II) atom of the latter forms three Sn···Se interactions to the three μ<sub>2</sub>-Se atoms of the cyclic core of the cation to form the zero-dimensional aggregate illustrated in Figure 2a. The interacting species in **2** [28] is the [NaSn<sub>12</sub>O<sub>8</sub>Se<sub>6</sub>]<sup>3−</sup> tri-anion and this self-associates about a center of inversion to form a dimeric aggregate mediated by two Sn···Se interactions as shown in Figure 2b. A three-molecule aggregate is observed in ionic **3** [29], Figure 2c. The non-symmetric, di-cation comprises of two bridged Sn<sub>3</sub>Se<sub>4</sub> cores, similar to that seen in **1**, and again similar to **1**; one μ<sub>2</sub>-Se atom of each core associates via a Sn···Se interaction with a tin(II) atom derived from a [SnCl<sub>3</sub>]<sup>−</sup> anion.

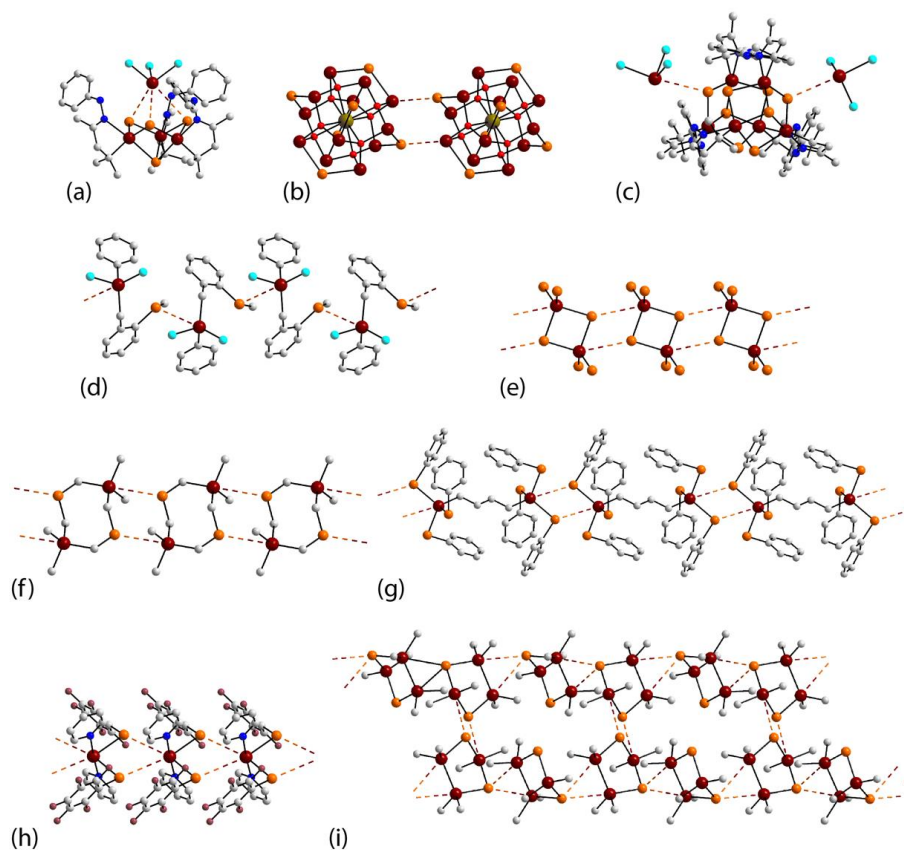


**Figure 2.** Supramolecular aggregation via Sn $\cdots$ Se secondary bonding in (a) **1** {UJAZIQ;  $d(\text{Sn}\cdots\text{Se}) = 3.76, 3.79 \text{ \AA} \text{ \& } 3.90 \text{ \AA}$ }, (b) **2** {PUZCUI;  $3.84 \text{ \AA}$ }, (c) **3** {BIFCAX;  $3.64 \text{ \AA} \text{ \& } 3.81 \text{ \AA}$ }, (d) **4** {BELCUS;  $3.65 \text{ \AA}$ }, (e) **5** {RESTER;  $3.77 \text{ \AA}$ }, (f) **7** {LEVLEE;  $3.88 \text{ \AA}$ }, (g) **8** {TORPOG;  $3.86 \text{ \AA}$ }, (h) **9** {WUSWOY;  $3.79 \text{ \AA}$ }, and (i) **10** {MESESN;  $3.77 \text{ \AA} \text{ \& } 3.91 \text{ \AA} \text{ \& } 3.84, 3.93 \text{ \AA} \text{ \& } 3.98 \text{ \AA}$ }. Color code in this and subsequent diagrams: main group element, brown; selenium, orange; chloride, cyan; fluoride, plum; oxygen, red; nitrogen, blue; and carbon, gray.

Seven of the tin compounds self-associate to form one-dimensional chains in their crystals, adopting varying topologies and numbers of Sn $\cdots$ Se interactions sustaining the chains. Compound **4** [30], the first example of a neutral compound and one containing a tin(IV) center, was investigated in terms of systematically varying the substitution pattern in molecules of the formula  $(2\text{-MeSeC}_6\text{H}_4\text{CH}_2)\text{Sn}(\text{Ph})_{3-n}\text{Cl}_n$ , and ascertaining supramolecular association patterns. In the case of **4**, that is with  $n = 2$ , molecules self-associate into a helical chain ( $2_1$  screw symmetry) via Sn $\cdots$ Se interactions, as shown in Figure 2d. The next two chains involve the association between tetra-anionic species,  $[\text{Sn}_2(\mu_2\text{-Se})_2\text{Se}_4]^{4-}$ , but the Sn $\cdots$ Se interactions involve the non-charged  $\mu_2\text{-Se}$  atoms. The compositions of **5** [31], Figure 2e, and **6** ([32]; SEKYEN) differ in the nature of the counter-cations. The tetra-anion in **5** is disposed about a center of inversion and is connected to centrosymmetrically related aggregates via two Sn $\cdots$ Se interactions and  $\{\text{Sn}\cdots\text{Se}\}_2$  synthons to form a linear, supramolecular tape. Essentially the same arrangement is observed in **6** where the  $\text{Sn}_2\text{Se}_2$  core lies on a mirror plane and is disposed about a center of inversion; the Sn $\cdots$ Se separation is  $4.02 \text{ \AA}$ . The neutral, cyclic compound **7** [33], is disposed about a center of inversion and also connects into a linear, supramolecular tape via Sn $\cdots$ Se interactions involving the  $\mu_2\text{-Se}$  atoms, Figure 2f. Binuclear **8** [34], where the tin(IV) atoms are bridged by a butyl chain, is disposed about a center of inversion and associates with inversion related molecules via  $\{\text{Sn}\cdots\text{Se}\}_2$  synthons, Figure 2g. In **9** [35], designed as a volatile synthetic precursor for SnSe nanomaterials, the tin(IV) atom lies on a 2-fold axis of

symmetry, a variation occurs in that the tin atom accepts two  $\text{Sn} \cdots \text{Se}$  interactions from a symmetry related molecule also on the 2-fold axis to form a twisted chain, Figure 2h. The crystallographic asymmetric unit of **10** comprises of two independent five-membered  $(\text{Me}_2\text{Sn})_3\text{Se}_2$  rings and these form distinct  $\text{Sn} \cdots \text{Se}$  interactions [36]. For the first independent molecule, only two of the constituent tin(IV) atoms, that is, the two tin atoms bonded to each other each forms a  $\text{Sn} \cdots \text{Se}$  interaction and one of the selenium atoms forms two contacts. In the second independent molecule, each of the tin(IV) atoms forms a single  $\text{Sn} \cdots \text{S}$  interaction, one selenium atom forms one contact and the other selenium atom participates in two  $\text{Sn} \cdots \text{Se}$  interactions. In the crystal, alternating independent molecules assemble into a chain, forming comparable  $\text{Sn} \cdots \text{Se}$  interactions involving the bonded tin atoms connecting to the selenium atoms that form two  $\text{Sn} \cdots \text{Se}$  contacts. Centrosymmetrically related chains associate via  $\{\text{Sn} \cdots \text{Se}\}_2$  synthons involving the second independent molecule only. The resultant double-chain is illustrated in Figure 2i.

The remaining three tin structures assemble into higher-dimensional arrays. In binuclear and centrosymmetric **11** [37], designed as a precursor for the chemical vapor deposition of SnSe nanomaterials, each of the tin(II) atoms forms a single  $\text{Sn} \cdots \text{Se}$  interaction as does one of the two independent selenium atoms. As these extend laterally, a two-dimensional array results with a corrugated topology, as seen in the views of Figure 3a. In binuclear **12** [38], the molecule is disposed about a 2-fold axis of symmetry and has a twisted, U-shape. Each of the tin(IV) and selenium atoms participates in a  $\text{Sn} \cdots \text{Se}$  interaction to form the corrugated array of Figure 3b.

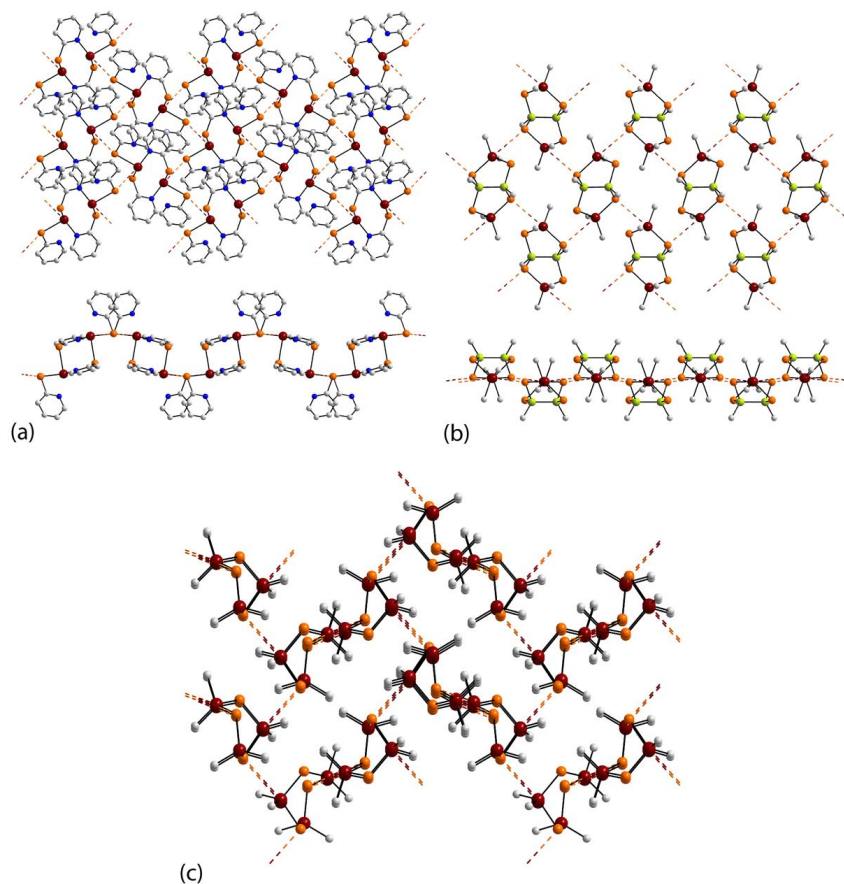


**Figure 3.** Supramolecular aggregation via  $\text{Sn} \cdots \text{Se}$  secondary bonding in (a) **11** [ZOPWIK;  $d(\text{Sn} \cdots \text{Se}) = 3.62 \text{ \AA}$ ], (b) **12** [UCORE];  $4.01 \text{ \AA}$ ], and (c) **13** [HMCTSS;  $4.01 \text{ \AA}$ ]. Additional color code: silicon, olive-green.

The cyclic, trinuclear molecule  $(\text{Me}_2\text{Sn})_3\text{Se}_3$  in **13** [39] has one pair of the diagonally opposite tin(IV) and selenium atoms lying on a 2-fold axis of symmetry, with the ring-atoms not lying on the axis each participating in a single  $\text{Sn}\cdots\text{Se}$  interaction. These interactions extend in three-dimensions to consolidate the molecular packing, Figure 3c.

### 3.2. Lead Compounds Featuring $\text{Pb}\cdots\text{Se}$ Interactions in Their Crystals

There are seven lead compounds satisfying the specified search criteria, **14–20**, and the chemical diagrams for the interacting species in these are shown in Figure 4. The common feature of each structure is the +II oxidation state for the lead atom so all  $\text{Pb}\cdots\text{Se}$  interactions can be classified as tetrel bonding interactions. Three of the molecules self-associate to form zero-dimensional aggregates and the remaining examples form one-dimensional chains in their crystals.

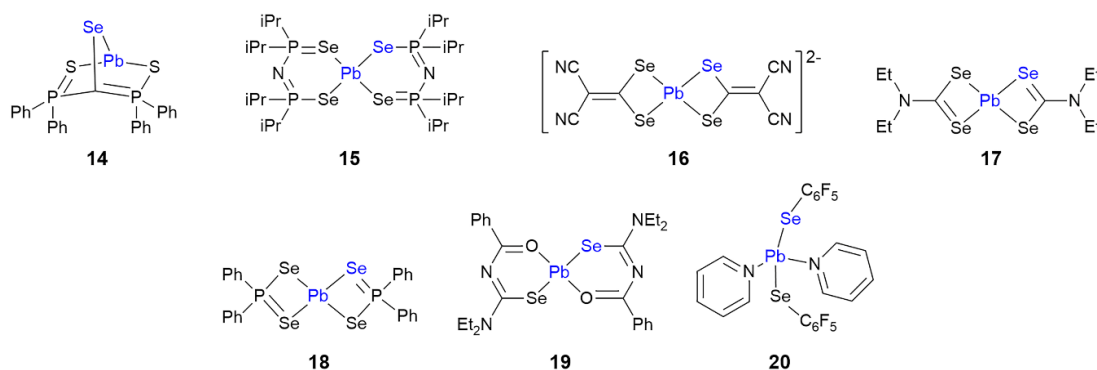
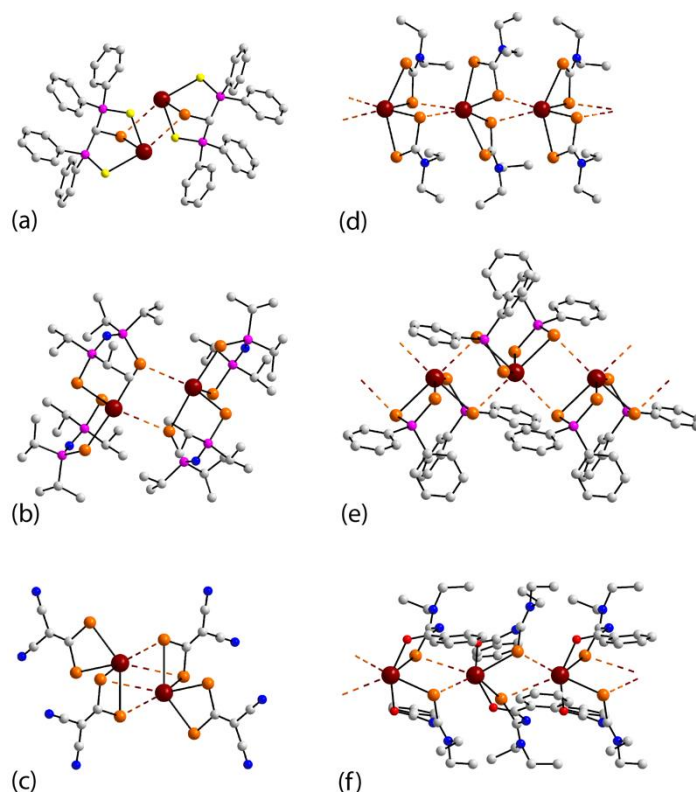


Figure 4. Chemical diagrams for lead compounds 14–20.

The first aggregate is the centrosymmetric dimer formed by **14** [40] which was developed as a precursor for the chemical vapor deposition (CVD) of PbSe nanoparticles. As shown in Figure 5a, molecules associate through two  $\text{Pb}\cdots\text{Se}$  interactions via a  $\{\text{Pb}-\text{Se}\cdots\}_2$  synthon. A similar  $\{\text{Pb}-\text{Se}\cdots\}_2$  synthon is found in **15** [41], Figure 5b, but the dimeric aggregate has crystallographic 2-fold symmetry. The di-anion in **16** [42], which thermally decomposes to PbSe, associates about a center of inversion with each of the selenium atoms of one 2,2-dicyano-ethylene-1,1-diselenolate ligand forming  $\text{Pb}\cdots\text{Se}$  interactions, Figure 5c. The remaining molecules in this section associate to form one-dimensional chains.

In **17** [43], developed as a synthetic precursor for PbSe nanomaterials, a selenium atom of each of the asymmetrically chelating diselenocarbamate ligands connects to the same symmetry related lead(II) atom; as a result, a zigzag chain is formed (glide symmetry), Figure 5d. One selenium atom of each of the asymmetrically coordinating diselenophosphinate ligands in **18** [44] also forms a  $\text{Pb}\cdots\text{Se}$  interaction but with different centrosymmetrically related molecules, leading to the formation of a twisted supramolecular chain sustained by  $\{\text{Pb}-\text{Se}\cdots\}_2$  synthons, Figure 5e. The compound was prepared in the context of investigating the mechanism of forming quantum dots from tertiary phosphine selenide sources. The lead(II) atom in **19** [45] lies on a 2-fold axis of symmetry and the coordinated selenium atoms associate with the same symmetry related lead(II) atom to form a twisted, supramolecular chain, Figure 5f. The structure of **20** [35] is isostructural with the tin(II) analog, **9**, described as a twisted chain and illustrated in Figure 2h; **9** was investigated for its utility as a single source precursor for PbSe nanoparticles.



**Figure 5.** Supramolecular aggregation via Pb $\cdots$ Se secondary bonding in (a) **14** {UTAJUV; d(Pb $\cdots$ Se) = 3.41 Å}, (b) **15** {TAKLOI; 3.57 Å}, (c) **16** {KUHSAH; 3.49 & 3.72 Å}, (d) **17** {BOKMUJ; 3.47 & 3.62 Å}, (e) **18** {XUZTUI; 3.27 & 3.40 Å}, and (f) **19** {YIBHOG; 3.64 Å}. Additional color code: phosphorus, pink.

### 3.3. Arsenic Compounds Featuring As $\cdots$ Se Interactions in their Crystals

A relatively small number of compounds featuring As $\cdots$ Se interactions in their crystals are known and the chemical structures for the interacting species are shown in Figure 6, that is for **21–27**, and, as demonstrated above, even though there is only a small number of examples, there is a great diversity in supramolecular architectures.

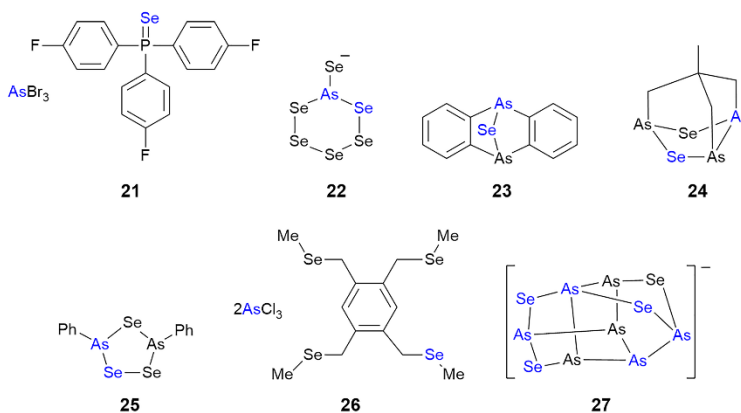


**Figure 6.** Chemical diagrams for arsenic compounds **21–27**.

The first selenide included in this survey is noted in the crystal of **21** [46], where two distinct molecules associate via As $\cdots$ Se interactions, with the participating atoms being arsenic(III) and selenide-selenium atoms, indicative of a pnictogen interaction. Each of the molecules is located on a crystallographic 3-fold axis of symmetry and associate with a crystallographic site of symmetry 23. It can be noted from the Figure 7a that each phosphaneselenide atom forms three As $\cdots$ Se interactions with three different AsBr<sub>3</sub> molecules so that a distorted As<sub>4</sub>Se<sub>4</sub> cube, sustained by eight As $\cdots$ Se interactions, defines the core of the aggregate. The mono-anion in **22** [47] has the charge localized on the exocyclic selenium atom with the dimeric aggregate in the crystal shown in Figure 7b sustained by As $\cdots$ Se interactions between centrosymmetrically related anions.

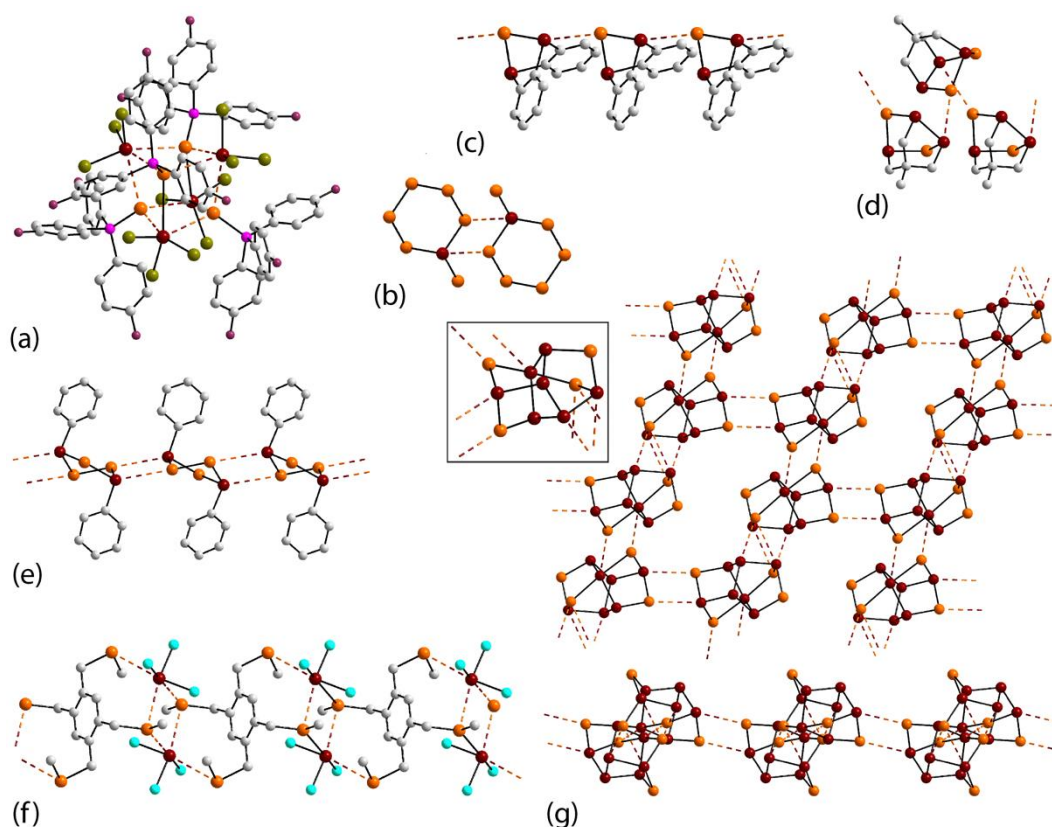


**Figure 7.** Supramolecular aggregation via As $\cdots$ Se secondary bonding in (a) **21** {GEXSOT;  $d(\text{As}\cdots\text{Se}) = 3.37$  Å}, (b) **22** {NEKJIW; 3.48 Å}, (c) **23** {ESEARS; 3.63 Å}, (d) **24** {COSDIX; 3.64 Å}, (e) **25** {SEDMAP; 3.53 Å}, (f) **26** {WAMCOE; 3.29, 3.42 & 3.60 Å}, and (g) **27** {KAXXUC; 3.60, 3.61, 3.64 & 3.72 Å}. Additional color code: bromide, olive-green.

There are four examples whereby one-dimensional chains are formed through As $\cdots$ Se interactions. In **23** [48], a mirror plane bisects the molecule with the selenium atom lying on the plane. The molecules are assembled into a linear chain via a single As $\cdots$ Se connection per molecule, Figure 7c. Similar connections are noted in the crystal of **24** [49], comprising a five-membered As<sub>3</sub>Se<sub>2</sub> ring, whereby only one of the three potential arsenic(III) atoms and one of the two selenium atoms are engaged in As $\cdots$ Se interactions to form a chain with a helical topology being propagated by 2<sub>1</sub>-screw symmetry, Figure 7d. A third topology for the chain is seen in the crystal of **25** [50] where the molecule is disposed about a 2-fold axis of symmetry. There are on average two As $\cdots$ Se interactions between the molecules and being propagated by glide symmetry; the chain has a zigzag topology, Figure 7e. The fourth one-dimensional architecture

observed for **26** [51] reverts to a helical topology ( $2_1$  screw symmetry), Figure 7f, but exhibits quite distinct features than for **24**. In the crystal, two  $\text{AsCl}_3$  molecules are bridged by two selenium atoms to form a  $\{\text{As}\cdots\text{Se}\}_2$  synthon. These are further connected by additional  $\text{As}\cdots\text{Se}$  interactions (3.42 Å) to form the helical, supramolecular chain. In this scheme, the arsenic(III) center participates in three  $\text{As}\cdots\text{Se}$  interactions as seen in **21** and in the next structure to be described, **27**.

A two-dimensional architecture is constructed in the crystal of **27** [52] as a result of three distinct  $\text{As}\cdots\text{Se}$  interactions. As is evident from the inset of Figure 7g, the mono-anion, formulated as  $\text{As}_7\text{Se}_4^-$ , participates in eight  $\text{As}\cdots\text{Se}$  interactions whereby four arsenic atoms form a single interaction, as do two of the selenium atoms with one selenium atom forming two  $\text{As}\cdots\text{Se}$  contacts. Three of the contacts involve directly bonded arsenic and selenium atoms and occur around a center of inversion in each case; thus, there are three independent  $\{\text{As}-\text{Se}\cdots\}_2$  synthons. The two remaining interactions occur between bonded arsenic atoms connecting to a single selenium atom, which thereby lead to the formation of a three-membered  $\{\cdots\text{AsAs}\cdots\text{Se}\}$  synthon. The result is the grid shown in Figure 7g, which define rather large voids that accommodate the tetraphenylphosphonium counter-cations.

### 3.4. Antimony Compounds Featuring $\text{Sb}\cdots\text{Se}$ Interactions in their Crystals

Eight crystals feature  $\text{Sb}\cdots\text{Se}$  interactions leading to zero-, one-, and two-dimensional aggregation patterns. The chemical diagrams for the interacting species in these, that is, **28–35**, are shown in Figure 8.

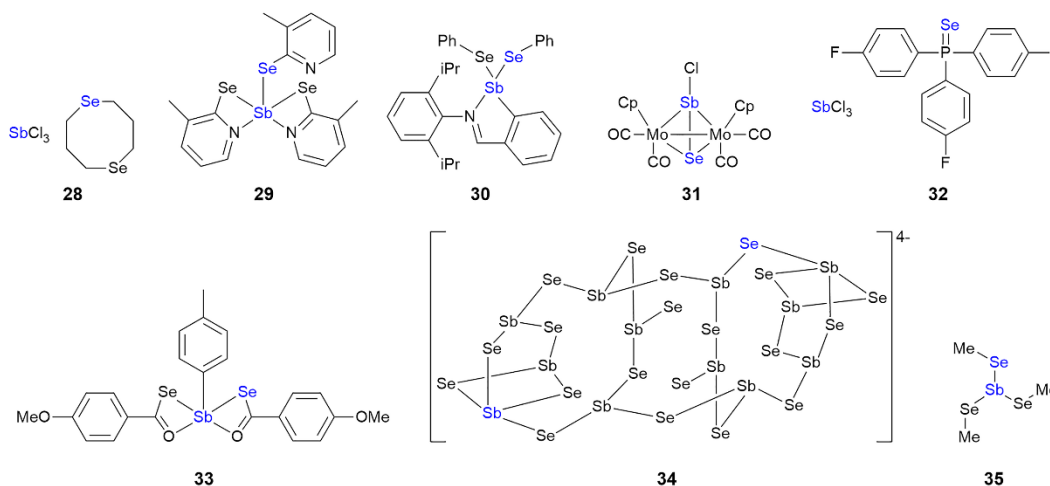


**Figure 8.** Chemical diagrams for antimony compounds **28–35**; Cp is cyclopentadienyl.

The supramolecular association in the crystal of **28** [53] is an illuminative example of cooperation between  $\text{Sb}\cdots\text{Se}$  and  $\text{Sb}\cdots\text{Cl}$  secondary bonding interactions. As evidenced from Figure 9a, there is a  $\text{Sb}\cdots\text{Se}$  interaction between the  $\text{SbCl}_3$  molecule and one of the selenium atoms of the eight-membered ring of the 1,5-diselenacyclooctane molecule. These aggregates associate about a center of inversion via  $\text{Sb}\cdots\text{Cl}$  interactions to form a four-molecule aggregate. The molecules in **29** [54], Figure 9b, **30** ([55]; KIMNEB;  $\text{Sb}\cdots\text{Se} = 3.69$  Å) and **31** ([56]; ISIEPEG  $\text{Sb}\cdots\text{Se} = 3.88$  Å) are centrosymmetric dimers sustained by two  $\text{Sb}\cdots\text{Se}$  interactions; **29** [54] was employed as a precursor for CVD of  $\text{Sb}_2\text{Se}_3$  and aerosol-assisted chemical vapor deposition (AACVD) of  $\text{Sb}_2\text{Se}_3$  thin films. The last zero-dimensional aggregate is found in the crystal of **32** ([46]; GEXSIN; 3.36 Å). This is centered about a distorted  $\text{Sb}_4\text{Se}_4$  cube, sustained by eight  $\text{Sb}\cdots\text{Se}$  interactions, as described above for isostructural **21** [46], Figure 7b.

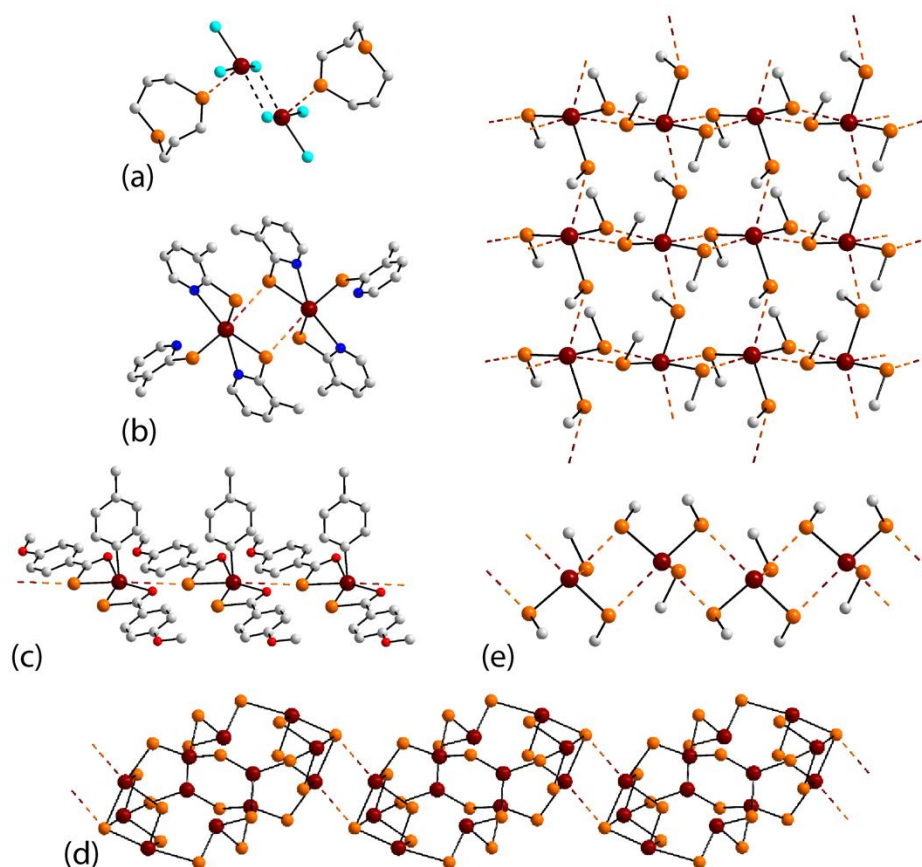


**Figure 9.** Supramolecular aggregation via Sb $\cdots$ Se secondary bonding in (a) **28** {EWIWI;  $d(\text{Sb}\cdots\text{Se}) = 3.29$  Å}, (b) **29** {TAKSEF; 3.67 Å}, (c) **33** {ACUPAQ; 3.87 Å}, (d) **34** {HEFCOK; 3.61 Å}, and (e) **35** {JAZGIA; 3.55, 3.64 & 3.66 Å}.

Two one-dimensional chains are sustained by Sb $\cdots$ Se interactions. There is an average of one Sb $\cdots$ Se interaction per repeat unit in **33** [57] where the resulting topology is linear and where the interacting selenium atom approaches the antimony atom within the O<sub>2</sub>Se<sub>2</sub> skewed-trapezoidal plane in the region between the two oxygen atoms, Figure 9c. The [Sb<sub>12</sub>Se<sub>20</sub>]<sup>4-</sup> Zintl ion in **34** [58] also self-associates into a linear chain whereby centrosymmetrically related tetra-anions are connected by a {Sb $\cdots$ Se}<sub>2</sub> synthon, Figure 9d.

The last crystal in this section to be discussed features the smallest molecule in this category, that is, Sb(SeMe)<sub>3</sub> in **35** [59]. Similar to that seen in **32**, the antimony atom accepts three Sb $\cdots$ Se interactions as each selenium atom participates in one such contact. To a first approximation, the resultant two-dimensional array has the form of a square grid and displays a corrugated topology, as seen in the views of Figure 9e.

### 3.5. Bismuth Compounds Featuring Bi $\cdots$ Se Interactions in their Crystals

There are only six bismuth-/selenium-containing crystals featuring Bi $\cdots$ Se interactions and the chemical structures of the interacting species in these, that is, **36–41**, are shown in Figure 10.

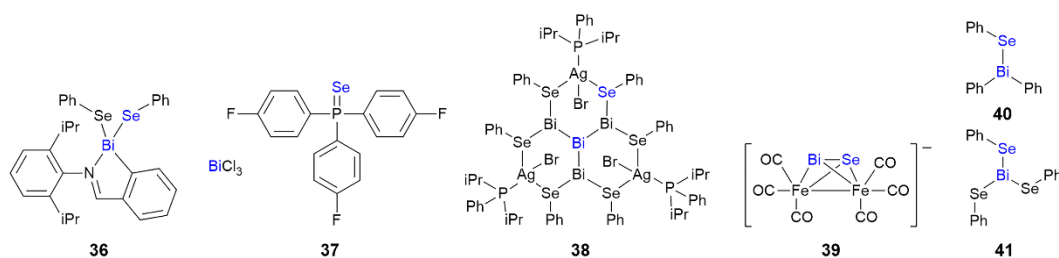


**Figure 10.** Chemical diagrams for bismuth compounds 36–41.

A simple dimeric aggregate sustained by two  $\text{Bi}\cdots\text{Se}$  interactions and a  $\{\text{Bi}-\text{Se}\cdots\}_2$  synthon is observed in the crystal of **36** [55]. While this has the appearance, at least to a first approximation, of several related species covered above (Figure 11a), the difference here is that the association is not through a center of inversion, as is usually observed. In this case, the contacts occur between two crystallographically independent molecules. The association in **37** ([46]; GEXSEJ; 3.35 Å), with a supramolecular  $\text{Bi}_4\text{Se}_4$  core sustained by  $\text{Bi}\cdots\text{S}$  interactions, is as described previously for **21**, Figure 7b, and **32**. An aesthetically pleasing  $\text{Bi}_4$  core is a key feature in the crystal of **38** [60], with each edge of the  $\text{Bi}_3$  triangle, which encompasses a central bismuth atom, being bridged by a sequence of  $\text{Se}-\text{Ag}-\text{Se}$  atoms. Centrosymmetrically related molecules associate through a center of inversion and are sustained by four  $\text{Bi}\cdots\text{Se}$  interactions, as is apparent from the two views of Figure 11b.

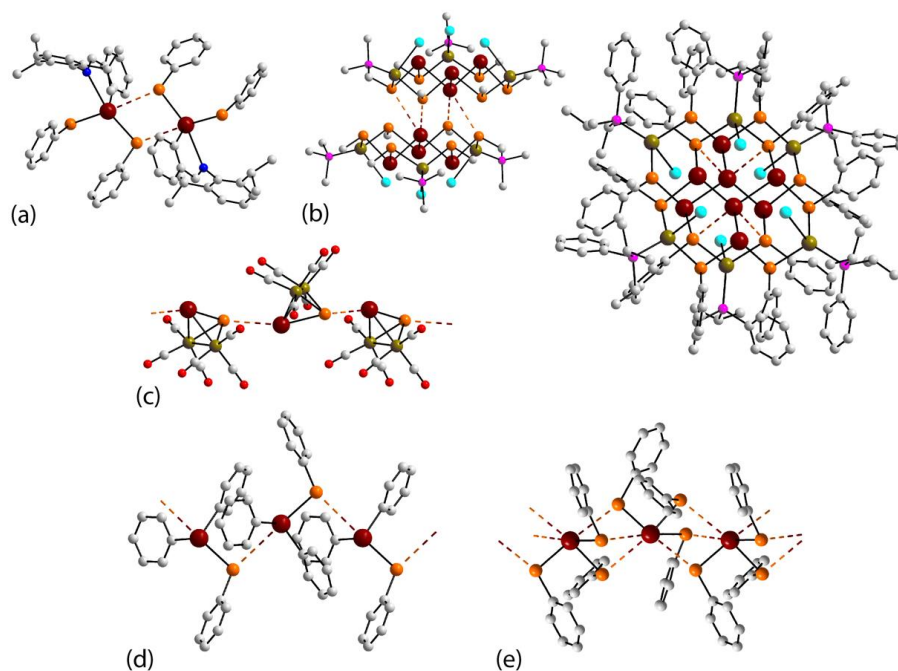


**Figure 11.** Supramolecular aggregation via  $\text{Bi}\cdots\text{Se}$  secondary bonding in (a) **36** [KIMMEA;  $d(\text{Bi}\cdots\text{Se}) = 3.51$  &  $3.55$  Å], (b) **38** [EGPEM;  $3.70$  &  $3.83$  Å], (c) **39** [COFGEM;  $3.48$  Å], (d) **40** [GIPREC;  $3.90$  Å], and (e) **41** [MIWFAA;  $3.48$ ,  $3.50$  &  $3.57$  Å]. Additional color code: silver and iron, dark-green.

The three remaining crystals feature one-dimensional chains. In **39** [61], of interest owing to a semi-conducting character and where a  $\text{Bi}-\text{Se}$  atom pair caps a  $\text{Fe}_2(\text{CO})_6$  unit, the presence of  $\text{Bi}\cdots\text{Se}$  interactions lead to a helical, supramolecular chain; Figure 11c. A helical chain is also observed in **40** [62], Figure 11d, again sustained by, on average one  $\text{Bi}\cdots\text{Se}$  interaction per repeat unit. When the

two bismuth-bound phenyl groups of **40** are replaced by two phenylselenenyl groups, leading to **41** [63], significantly more Bi···Se interactions are evident. The asymmetric unit of **41** comprises two independent molecules and each of these self-associates into a helical chain, as for **39** and **40**, but, in this case, there are, on average, three Bi···Se interactions per repeat unit in each of the independent chains formed in the crystal, one of which is illustrated in Figure 11e; the Bi···Se separations for the second independent chain are 3.49 and  $2 \times 3.59$  Å. This propensity to form Bi···Se interactions in Bi(SePh)<sub>3</sub> (**40**) is not pervasive as the structure suggests. For example, the molecule highlighted in **38** co-crystallizes with one equivalent of Bi(SePh)<sub>3</sub> as well as one equivalent of 1,2-dimethoxyethane (solvate). However, Bi(SePh)<sub>3</sub> in **38** (and in the disordered chloride analog of **38**) does not participate in Bi···Se interactions, instead the bismuth atom forms Bi···Br (Bi···Cl) secondary bonding interactions with the other bismuth-containing molecule.

### 3.6. Tellurium Compounds Featuring Te···Se Interactions in Their Crystals

The most numerous among the main group elements covered in the present survey are those having tellurium, with 17 examples. The chemical diagrams for **42**–**58** are given in Figure 12. As with the earlier series covered, herein a broad range of compounds and supramolecular motifs are noted.

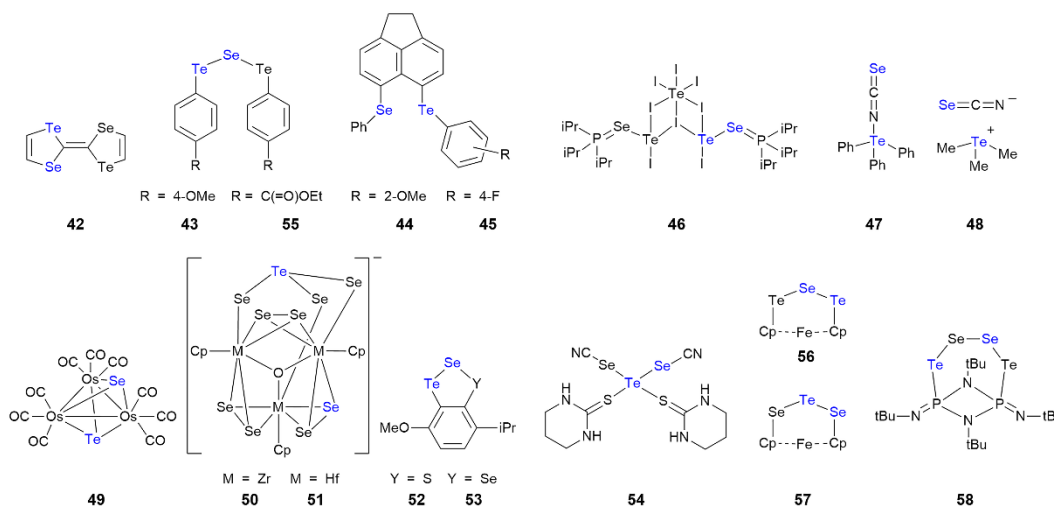


**Figure 12.** Chemical diagrams for tellurium compounds **42**–**58**; Cp is cyclopentadienyl.

Six of the compounds assemble into zero-dimensional motifs. In **42** [64], the tellurium and selenium atoms of one of the five-membered rings associate about a center of inversion to form the dimeric aggregate shown in Figure 13a. When **42** was cocrystallized with TCNQ (tetracyanoquinodimethane), highly conductive charge-transfer (CT) complexes were formed [64]. Similar centrosymmetric {Te–Se···}<sub>2</sub> synthons are observed in each of **43** [65], Figure 13b, **44** ([66], MIVYIB;  $d(\text{Te} \cdots \text{Se}) = 3.90$  Å), and **45** ([66], MIVZAU; 3.93 Å). Again, a {Te–Se···}<sub>2</sub> synthon is noted in **46** [67], Figure 13c, a compound that is particularly noteworthy for the relatively high number of potential iodide donors but, where Te···Se interactions prevail. The ion-pair in **47** [68] is formulated as [Ph<sub>3</sub>Te][N=C=S] with the closest association between the constituent species being Te···N contacts of 2.81 and 3.12 Å, represented as black dashed lines in Figure 13d, for the two independent ion-pairs comprising the asymmetric unit. In terms of Te···Se interactions, one of the two independent ion-pairs associates with a center of inversion via a {Te–Se···}<sub>2</sub> synthon. Associated with this are two of the second independent ion-pairs (each separated by 3.43 Å) so a four-ion-pair aggregate is generated. A related ion-pair, [Me<sub>3</sub>Te][N=C=S], is seen in **48** [68], where, consistent with the replacement of the tellurium-bound phenyl substituents of **47** with (relatively)

electropositive methyl substituents, the  $\text{Te}\cdots\text{N}$  separation is elongated to 3.25 Å. The constituents of the ion-pair are connected into a supramolecular chain with a zigzag topology via  $\text{Te}\cdots\text{Se}$  interactions, Figure 13e. When the weak  $\text{Te}\cdots\text{N}$  interactions are taken into consideration, the aforementioned chains are connected into a two-dimensional array (not illustrated).

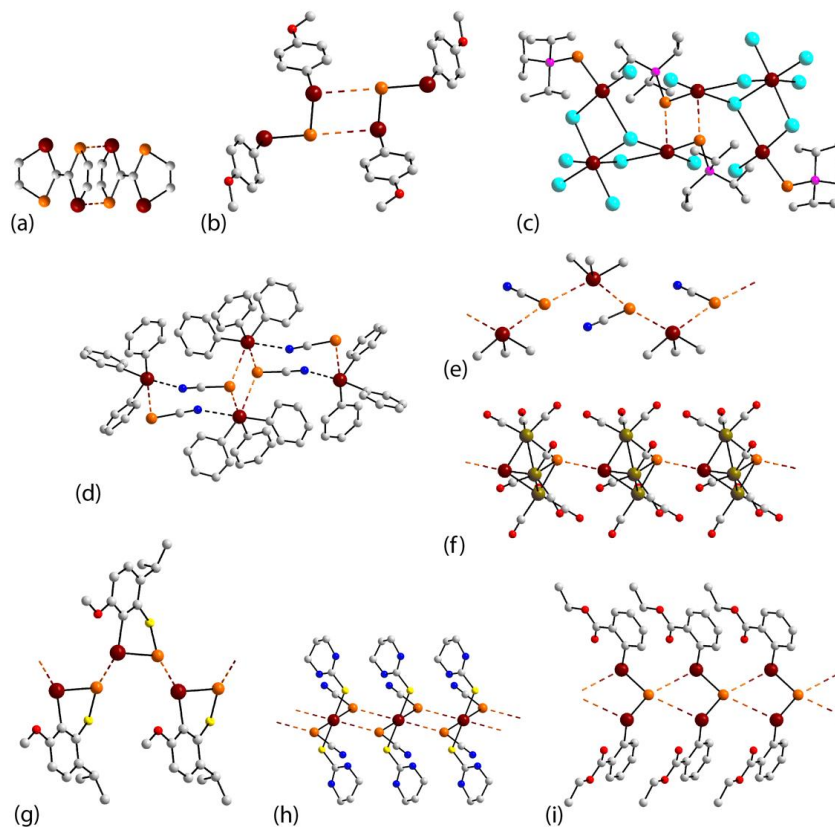


**Figure 13.** Supramolecular aggregation via  $\text{Te}\cdots\text{Se}$  secondary bonding in (a) **42** {ECITEP;  $d(\text{Te}\cdots\text{Se}) = 3.81$  Å}, (b) **43** {BAWFUA; 3.68 Å}, (c) **46** {YIKFOO; 3.74 Å}, (d) **47** {ZZZAIJ01; 3.43, 3.44 & 3.54 Å}, (e) **48** {HUHCIW; 3.47 & 3.55 Å}, (f) **49** {QENRIK; 3.95 Å}, (g) **52** {XOTLUN; 3.48 Å}, (h) **54** {TRTUTE; 3.82 Å}, and (i) **55** {BAWGAH; 3.84 Å}. Additional color code: osmium, dark-green; sulfur, yellow.

In cluster compound **49** [69], the osmium atoms of the  $\text{Os}_3(\text{CO})_9$  core are  $\mu_3$ -capped on either side by tellurium and selenium atoms, which associate in the crystal to form a linear, supramolecular chain with an average of one  $\text{Te}\cdots\text{Se}$  interaction per repeat unit, Figure 13f. In isostructural **50** and **51** [70], constructed about  $\text{M}_3\text{O}$  cores,  $\text{M} = \text{Zr}$  (**50**) and  $\text{Hf}$  (**51**), and featuring an unusual  $\text{TeSe}_3$  capping residue, molecules associate into helical chains ( $2_1$  screw symmetry) via  $\text{Te}\cdots\text{Se}$  interactions. Similar helical chains are observed in **52**, Figure 13g, and **53** [71], which differ in the nature of the atom connecting the aromatic ring to the selenium atom bonded to the tellurium atom, the latter associate to form the chain. On average, there are two  $\text{Te}\cdots\text{Se}$  interactions linking the repeat unit of **54** [72] where the tellurium is located on a center of inversion. The resulting chain has a linear topology, Figure 13h. Compound **55** [65] is closely related to that of **43** in that the methoxy substituents of the latter have replaced by ethoxycarboxyl groups; the central selenium atom in **55** lies in a 2-fold axis of symmetry. Whereas **43** self-associates into a dimer, Figure 13b, **55** self-associates into a linear, supramolecular chain as each selenium atom forms two  $\text{Te}\cdots\text{Se}$  interactions with a translationally related molecule, Figure 13i.

Compound **56** [73] self-associates into a supramolecular chain, Figure 14a. Two independent molecules comprise the asymmetric unit and these differ in the number of Te $\cdots$ Se interactions they form. For the first independent molecule, one tellurium and the selenium atom form a single Te $\cdots$ Se interaction each, whereas for the second molecule, the same situation pertains, except both participating atoms form two Te $\cdots$ Se interactions. The connections between the independent molecules lead to a linear, supramolecular chain. Centrosymmetrically chains are linked into a double-chain via additional Te $\cdots$ Se interactions formed by the second independent molecule. The molecule in **57** [74] is related to that in **56** in that there has been an exchange between selenium and tellurium atoms. This results in a distinct supramolecular assembly. Here, the central tellurium atom forms two Te $\cdots$ Se interactions with each of the selenium atoms forming a single Te $\cdots$ Se interaction. These extend laterally so a two-dimensional array eventuates, Figure 14b. A comparison of the simplified images in Figure 14a,b highlight the different modes of association between molecules. The energies associated with individual Te $\cdots$ Se contacts were calculated for each of **56** and **57**, and for the latter, these were  $-10.8$  and  $-11.8$  kJ mol $^{-1}$  [74]. The molecule in **58** [75] features a seven-membered ring containing a string of Te–Se–Se–Te atoms bridged by a P–N–P link, the latter being a part of a four-membered N $_2$ P $_2$  ring. Each of the tellurium and selenium atoms forms a Te $\cdots$ Se interaction. Again, these extend laterally to form a two-dimensional array, Figure 14c.

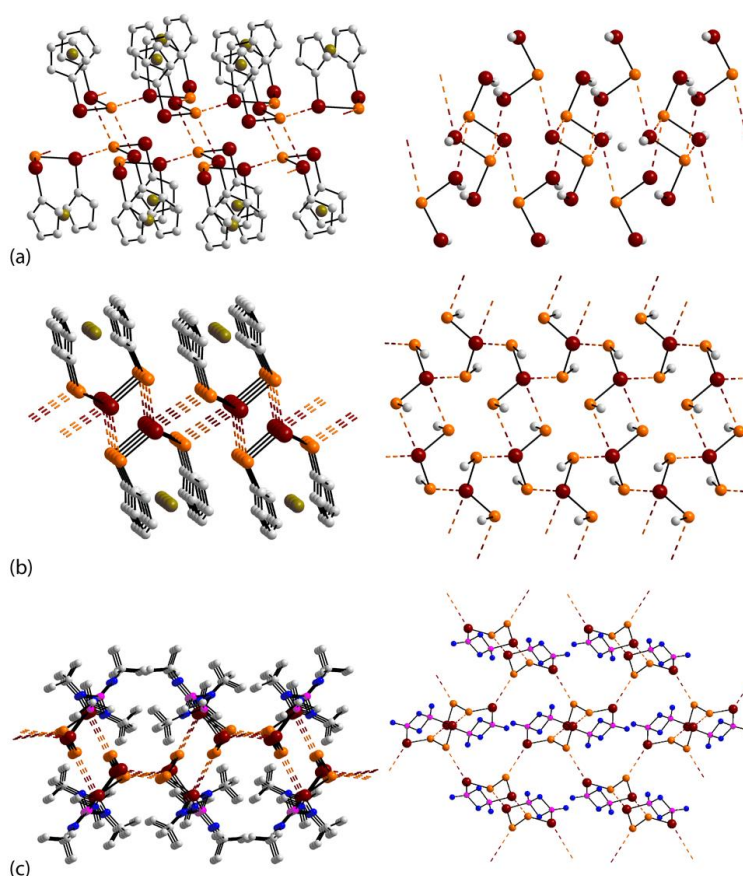


**Figure 14.** Supramolecular aggregation via Te $\cdots$ Se secondary bonding in (a) **56** {QAZGUV;  $d(\text{Te}\cdots\text{Se}) = 3.70, 3.79$  &  $3.92$  Å}, (b) **57** {OMIHAV;  $3.62$  &  $3.69$  Å}, and (c) **58** {ONEGIZ;  $3.82$  &  $3.89$  Å}. In the simplified views of (a) and (b), only the carbon atom bound to selenium/tellurium are shown, and in (c), the t-butyl groups are omitted.

#### 4. Discussion and Outlook

The foregoing describes 58 crystals featuring  $M \cdots Se$  secondary bonding interactions between main group elements (M) and selenium for  $M = Sn$  (13 examples),  $Pb$  (7),  $As$  (7),  $Sb$  (8),  $Bi$  (6), and  $Te$  (17). The percentage adoption of  $M \cdots Se$  in the crystals varies considerably. For example, of the 27 crystals containing both lead and selenium, seven feature  $Pb \cdots Se$  interactions, giving a percentage adoption of 26%. This falls off to 16% for bismuth to 10% for tellurium and then 6% (arsenic) and 5% (tin and antimony). One reason for the low adoption rates relates to the observation that secondary bonding interactions are extremely sensitive to steric hindrance—bulky groups present on the organometal center and/or ligands bound to the metal can preclude the formation of secondary bonding interactions [15–23]; steric considerations have been exploited for the rational design of coordination polymers in zinc and cadmium dithiolate chemistry [76]. In most of the crystals, the metal center forms a single  $M \cdots Se$  contact with few examples of the metal forming two contacts and rarely, three  $M \cdots Se$  contacts. With the formation of primarily one  $M \cdots Se$  interaction, the supramolecular architectures sustained by these interactions are usually zero- or one-dimensional, being found in 38 and 50% of all crystals, respectively. Two-dimensional architectures sustained by  $M \cdots Se$  interactions are found in 10% of the crystals and there is a single example of a three-dimensional architecture. A comment on the likely bonding responsible for the  $M \cdots Se$  interactions is appropriate. For the  $Sn \cdots S$  contacts, the majority features tin(IV) centers and so the interactions can be considered in terms of classic Lewis Acid/Lewis Base electrostatics. In contrast, all of the  $Pb \cdots Se$  contacts can be rationalized in terms of tetrel bonding; the overwhelming majority of  $M \cdots Se$  interactions formed by arsenic-triad arise from pnictogen bonding and the tellurium examples in terms of chalcogen bonding where  $\sigma$ -hole considerations come to the fore. Thus far, limited mention has been made of the energy of stabilization provided by  $M \cdots Se$  interactions. This is because supporting computational chemistry is largely lacking for  $M \cdots Se$  interactions with the exception of 56 and 57 [74]. However, in a recent commentary on supramolecular association involving metal centers, it was concluded that the energies of stabilization provided by various secondary bonding interactions was in the same range and often exceeded the energy of stabilization provided by conventional hydrogen bonding interactions [77]. This conclusion is emphasized in the very recently published analysis of a tetrel,  $C \cdots O$ , bond formed between a  $sp^3$ -carbon center and the oxygen atom of a tetrahydrofuran molecule, not an interaction that might be expected to be particularly notable, for which an energy of stabilization of about  $11 \text{ kcal mol}^{-1}$  was calculated [78]. In the context of the foregoing survey of  $M \cdots Se$  interactions, with diverse bonding circumstances and supramolecular molecular aggregation patterns, clearly there is enormous scope for further experimental work supported by theoretical analysis.

**Funding:** Crystallographic research at Sunway University is supported by Sunway University Sdn Bhd (Grant no. STR-RCTR-RCCM-001-2019).

**Conflicts of Interest:** The author declares no conflict of interest.

#### References

1. Minyaev, R.M.; Minkin, V.I. Theoretical study of  $O \rightarrow X$  (S, Se, Te) coordination in organic compounds. *Can. J. Chem.* **1998**, *76*, 776–778. [CrossRef]
2. Wang, W.; Ji, B.; Zhang, Y. Chalcogen bond: A sister noncovalent bond to halogen bond. *J. Phys. Chem. A* **2009**, *113*, 8132–8135. [CrossRef] [PubMed]
3. Aakeröy, C.B.; Bryce, D.L.; Desiraju, G.R.; Frontera, A.; Legon, A.C.; Nicotra, F.; Rissanen, K.; Scheiner, S.; Terraneo, G.; Metrangolo, P.; et al. Definition of the chalcogen bond (IUPAC Recommendations 2019). *Pure Appl. Chem.* **2019**, *91*, 1889–1892. [CrossRef]
4. Alkorta, I.; Elguero, J.; Frontera, A. Not only hydrogen bonds: Other noncovalent interactions. *Crystals* **2020**, *10*, 180. [CrossRef]

5. Bent, H.A. Structural chemistry of donor-acceptor interactions. *Chem. Rev.* **1968**, *68*, 587–648. [[CrossRef](#)]
6. Hassel, O. Structural Aspects of interatomic charge-transfer bonding. *Science* **1970**, *170*, 497–502. [[CrossRef](#)]
7. Alcock, N.W. Secondary bonding to nonmetallic elements. *Adv. Inorg. Chem. Radiochem.* **1972**, *15*, 1–58. [[CrossRef](#)]
8. Llaguno, E.C.; Paul, I.C. Crystal structure of a [1,2,5]oxaselenazolo[2,3-*b*][1,2,5]oxaselenazole-7-*Se*IV: A molecule with ‘short’ intramolecular Se . . . O distances, or ‘long’ Se–O bonds. *J. Chem. Soc. Perkin Trans.* **1972**, *2*, 2001–2006. [[CrossRef](#)]
9. Murray, J.S.; Lane, P.; Clark, T.; Politzer, P.  $\sigma$ -hole bonding: Molecules containing group VI atoms. *J. Mol. Model.* **2007**, *13*, 1033–1038. [[CrossRef](#)]
10. Politzer, P.; Murray, J.S.; Clark, T. Halogen bonding: An electrostatically-driven highly directional noncovalent interaction. *Phys. Chem. Chem. Phys.* **2010**, *12*, 7748–7757. [[CrossRef](#)]
11. Politzer, P.; Murray, J.S. Halogen bonding and other  $\sigma$ -hole interactions: A perspective. *Phys. Chem. Chem. Phys.* **2013**, *15*, 11178–11189. [[CrossRef](#)] [[PubMed](#)]
12. Bauzá, A.; Mooibroek, T.J.; Frontera, A. The bright future of unconventional  $\sigma/\pi$ -hole interactions. *ChemPhysChem* **2015**, *16*, 2496–2517. [[CrossRef](#)] [[PubMed](#)]
13. Kolar, M.H.; Hobza, P. Computer modeling of halogen bonds and other  $\sigma$ -hole interactions. *Chem. Rev.* **2016**, *116*, 5155–5187. [[CrossRef](#)] [[PubMed](#)]
14. Politzer, P.; Murray, J.S.  $\sigma$ -Hole interactions: Perspectives and misconceptions. *Crystals* **2017**, *7*, 212. [[CrossRef](#)]
15. Tiekink, E.R.T. Molecular architecture and supramolecular association in the zinc-triad 1,1-dithiolates. Steric control as a design element in crystal engineering? *CrystEngComm* **2003**, *5*, 101–113. [[CrossRef](#)]
16. Lai, C.S.; Tiekink, E.R.T. Structural diversity in the mercury(II) bis(*N,N*-dialkyldithiocarbamate) compounds: An example of the importance of considering crystal structure when rationalising molecular structure. *Z. Kristallogr. Cryst. Mater.* **2007**, *222*, 532–538. [[CrossRef](#)]
17. Tiekink, E.R.T. Exploring the topological landscape exhibited by binary zinc-triad 1,1-dithiolates. *Crystals* **2018**, *8*, 292. [[CrossRef](#)]
18. Buntine, M.A.; Kosovel, F.J.; Tiekink, E.R.T. Supramolecular Sn . . . Cl associations in diorganotin dichlorides and their influence on molecular geometry as studied by *ab initio* molecular orbital calculations. *CrystEngComm* **2003**, *5*, 331–336. [[CrossRef](#)]
19. Tiekink, E.R.T. Tin dithiocarbamates: Applications and structures. *Appl. Organomet. Chem.* **2008**, *22*, 533–550. [[CrossRef](#)]
20. Liu, Y.; Tiekink, E.R.T. Supramolecular associations in binary antimony(III) dithiocarbamates: Influence of ligand steric bulk, influence on coordination geometry, and competition with hydrogenbonding. *CrystEngComm* **2005**, *7*, 20–27. [[CrossRef](#)]
21. Tiekink, E.R.T. Aggregation patterns in the crystal structures of organometallic Group XV 1,1-dithiolates: The influence of the Lewis acidity of the central atom, metal- and ligand-bound steric bulk, and coordination potential of the 1,1-dithiolate ligands upon supramolecular architecture. *CrystEngComm* **2006**, *8*, 104–118. [[CrossRef](#)]
22. Lee, S.M.; Heard, P.J.; Tiekink, E.R.T. Molecular and supramolecular chemistry of mono- and di-selenium analogues of metal dithiocarbamates. *Coord. Chem. Rev.* **2018**, *375*, 410–423. [[CrossRef](#)]
23. Tiekink, E.R.T.; Zukerman-Schpector, J. Stereochemical activity of lone pairs of electrons and supramolecular aggregation patterns based on secondary interactions involving tellurium in its 1,1-dithiolate structures. *Coord. Chem. Rev.* **2010**, *254*, 46–76. [[CrossRef](#)]
24. Taylor, R.; Wood, P.A. A million crystal structures: The whole is greater than the sum of its parts. *Chem. Rev.* **2019**, *119*, 9427–9477. [[CrossRef](#)]
25. Bruno, I.J.; Cole, J.C.; Edgington, P.R.; Kessler, M.; Macrae, C.F.; McCabe, P.; Pearson, J.; Taylor, R. New software for searching the Cambridge Structural Database and visualizing crystal structures. *Acta Crystallogr. Sect. B Struct. Sci. Cryst. Eng. Mater.* **2002**, *58*, 389–397. [[CrossRef](#)]
26. DIAMOND, Version 3.2k; K. Brandenburg & M. Berndt GbR: Bonn, Germany, 2006.

27. Rinn, N.; Eußner, J.P.; Kaschuba, W.; Xie, X.; Dehnen, S. Formation and reactivity of organo-functionalized tin selenide clusters. *Chem. Eur. J.* **2016**, *22*, 3094–3104. [[CrossRef](#)]
28. Krautscheid, H.; Schmidtke, M.  $[\text{NaSn}_{12}\text{O}_8\text{Se}_6]^{3-}$ —ein chalcogenostannatanion mit schalenförmigem Aufbau. *Z. Anorg. Allg. Chem.* **2002**, *628*, 913–914. [[CrossRef](#)]
29. Dehnen, S.; Hanau, K.; Rinn, N.; Argentari, M. Organotin selenide clusters and hybrid capsules. *Chem. Eur. J.* **2018**, *24*, 11711–11716. [[CrossRef](#)]
30. Metta-Magaña, A.J.; Lopez-Cardoso, M.; Vargas, G.; Pannell, K.H. Major distinctions in the molecular and supramolecular structures of selenium-containing organotins,  $(o\text{-MeSe-C}_6\text{H}_4\text{CH}_2)\text{SnPh}_{3-n}\text{Cl}_n$  ( $n = 0, 1, 2$ ). *Z. Anorg. Allg. Chem.* **2012**, *638*, 1677–1682. [[CrossRef](#)]
31. Santner, S.; Sprenger, J.A.P.; Finze, M.; Dehnen, S. The role of  $[\text{BF}_4]^-$  and  $[\text{B}(\text{CN})_4]^-$  anions in the ionothermal synthesis of chalcogenidometalates. *Chem. Eur. J.* **2018**, *24*, 3474–3480. [[CrossRef](#)]
32. Kim, K.-W. DMF Solvothermal synthesis and structural characterization of  $[\text{dabcoH}]_2[(\text{CH}_3)_2\text{NH}_2]_2[\text{Sn}_2\text{Se}_6]$  DMF. *J. Korean Chem. Soc.* **2005**, *49*, 603–608. [[CrossRef](#)]
33. Block, E.; Dikarev, E.V.; Glass, R.S.; Jin, J.; Li, B.; Li, X.; Zhang, S.-Z. Synthesis, structure, and chemistry of new, mixed group 14 and 16 heterocycles: Nucleophile-induced ring contraction of mesocyclic dications. *J. Am. Chem. Soc.* **2006**, *128*, 14949–14961. [[CrossRef](#)] [[PubMed](#)]
34. Nayek, H.P.; Niedermeyer, H.; Dehnen, S. Preparation and conformation of organo-bridged bis[tris(arylchalcogenolato)tin] compounds—an experimental and quantum chemical study. *Z. Anorg. Allg. Chem.* **2008**, *634*, 2805–2810. [[CrossRef](#)]
35. Holligan, K.; Rogler, P.; Rehe, D.; Pamula, M.; Kornienko, A.Y.; Emge, T.J.; Krogh-Jespersen, K.; Brennan, J.G. Copper, indium, tin, and lead complexes with fluorinated selenolate ligands: Precursors to  $\text{MSe}_x$ . *Inorg. Chem.* **2015**, *54*, 8896–8904. [[CrossRef](#)] [[PubMed](#)]
36. Dräger, M.; Mathiasch, B. Kristallstrukturbestimmung und schwingungsanalyse von 2,2,4,4,5,5-hexamethyl-1,3-diselena-2,4,5-tristannolan  $\text{Se}_2\text{Sn}_3(\text{CH}_3)_6$ . *Z. Anorg. Allg. Chem.* **1980**, *470*, 45–58. [[CrossRef](#)]
37. Cheng, Y.; Emge, T.J.; Brennan, J.G. Pyridineselenolate Complexes of tin and lead:  $\text{Sn}(2\text{-SeNC}_5\text{H}_4)_2$ ,  $\text{Sn}(2\text{-SeNC}_5\text{H}_4)_4$ ,  $\text{Pb}(2\text{-SeNC}_5\text{H}_4)_2$ , and  $\text{Pb}(3\text{-Me}_3\text{Si-2-SeNC}_5\text{H}_3)_2$ . Volatile CVD precursors to Group IV–Group VI semiconductors. *Inorg. Chem.* **1996**, *35*, 342–346. [[CrossRef](#)]
38. Herzog, U.; Böhme, U.; Brendler, E.; Rheinwald, G. Group 14 chalcogenides featuring a bicyclo[3.3.0]octane skeleton. *J. Organomet. Chem.* **2001**, *630*, 139–148. [[CrossRef](#)]
39. Dräger, M.; Blecher, A.; Jacobsen, H.-J.; Krebs, B. Molekül- und kristallstruktur von hexamethylcyclo-tristannaselenan  $[(\text{CH}_3)_2\text{SnSe}]_3$ . *J. Organomet. Chem.* **1978**, *161*, 319–325. [[CrossRef](#)]
40. Leung, W.-P.; Wan, C.-L.; Kan, K.-W.; Mak, T.C.W. Synthesis, structure, and reactivity of Group 14 bis(thiophosphinoyl) metal complexes. *Organometallics* **2010**, *29*, 814–820. [[CrossRef](#)]
41. Ritch, J.S.; Chivers, T.; Ahmad, K.; Afzaal, M.; O'Brien, P. Synthesis, structures, and multinuclear NMR spectra of tin(II) and lead(II) complexes of tellurium-containing imidodiphosphate ligands: Preparation of two morphologies of phase-pure PbTe from a single-source precursor. *Inorg. Chem.* **2010**, *49*, 1198–1205. [[CrossRef](#)]
42. Hummel, H.-U.; Fischer, E.; Fischer, T.; Gruß, D.; Franke, A.; Dietzsch, W. Synthesen, strukturen und thermische abbaureaktionen von  $\text{Tl}^{\text{I}}$ -,  $\text{Pb}^{\text{II}}$ - und  $\text{Se}^{\text{II}}$ -komplexen mit 2,2-dicyanethylen-1,1-diselenolat. *Chem. Ber.* **1992**, *125*, 1565–1570. [[CrossRef](#)]
43. Trindade, T.; Monteiro, O.C.; O'Brien, P.; Motevalli, N. Synthesis of PbSe nanocrystallites using a single-source method. The X-ray crystal structure of lead (II) diethyldiselenocarbamate. *Polyhedron* **1999**, *18*, 1171–1175. [[CrossRef](#)]
44. Evans, C.M.; Evans, M.E.; Krauss, T.D. Mysteries of TOPSe revealed: Insights into quantum dot nucleation. *J. Am. Chem. Soc.* **2010**, *132*, 10973–10975. [[CrossRef](#)] [[PubMed](#)]
45. Schuster, M.; Bensch, W. (Se,O)-Koordinierte komplexe niedervalenter hauptgruppenmetalle: Die kristallstruktur von bis(N,N-diethyl-N'-benzoylselenoureato)blei(II). *Z. Naturforsch. B Chem. Sci.* **1994**, *49*, 1615–1619. [[CrossRef](#)]
46. Alhanash, F.B.; Barnes, N.A.; Brisdon, A.K.; Godfrey, S.M.; Pritchard, R.G. Formation of  $\text{M}_4\text{Se}_4$  cuboids ( $\text{M} = \text{As}, \text{Sb}, \text{Bi}$ ) via secondary pnictogen–chalcogen interactions in the co-crystals  $\text{MX}_3\cdot\text{Se}=\text{P}(\text{p-FC}_6\text{H}_4)_3$  ( $\text{M} = \text{As}, \text{X} = \text{Br}; \text{M} = \text{Sb}, \text{X} = \text{Cl}; \text{M} = \text{Bi}, \text{X} = \text{Cl}, \text{Br}$ ). *Dalton Trans.* **2012**, *41*, 10211–10218. [[CrossRef](#)]

47. Czado, W.; Müller, U. Cyclische polyselenidoarsenate(III) und -antimonate(III):  $\text{PPh}_4[\text{Se}_5\text{AsSe}]$ ,  $\text{PPh}_4[\text{AsSe}_{6-x}\text{S}_x]$ ,  $(\text{PPh}_4)_2[\text{As}_2\text{Se}_6] \cdot 2\text{CH}_3\text{CN}$  und  $(\text{PPh}_4)_2[\text{Se}_6\text{SbSe}]_2$ . *Z. Anorg. Allg. Chem.* **1998**, *624*, 239–243. [[CrossRef](#)]
48. Kennard, O.; Wampler, D.L.; Coppola, J.C.; Motherwell, W.D.S.; Mann, F.G.; Watson, D.G.; MacGillavry, C.H.; Stam, C.H.; Benci, P. Crystal and molecular structure of 5,10-epoxy-, 5,10-epithio-, 5,10-episeleno-, and 5,10-epitelluro-5,10-dihydroarsanthren. *J. Chem. Soc. C* **1971**, 1511–1515. [[CrossRef](#)]
49. Thiele, G.; Rotter, H.W.; Lietz, M.; Ellermann, J. Chemistry of polyfunctional molecules, 80 [1] Crystal and molecular structures of the heteronoradamantanes 5-methyl-2.2.8.8-tetra-ethoxycarbonyl-1.3.7-triarsa-tricyclo[3.3.1.0<sup>3,7</sup>]nonane and 5-methyl-1.3.7-triarsa-2.8-diselena-[3.3.1.0<sup>3,7</sup>]nonane. *Z. Naturforsch. B Chem. Sci.* **1984**, *39*, 1344–1349. [[CrossRef](#)]
50. Applegate, C.A.; Meyers, E.A.; Zingaro, R.A.; Merijanjan, A. reactions of arsenic and arsonic acids with  $\text{H}_2\text{S}$  and  $\text{H}_2\text{Se}$ : Crystal structure of 1,4-diphenyl-1,4-diarsa-2,3,5-triselenacyclopentane. *Phosphorus Sulfur Rel. Elements* **1988**, *35*, 363–370. [[CrossRef](#)]
51. Levason, W.; Maheshwari, S.; Ratnani, R.; Reid, G.; Webster, M.; Zhang, W. Structural diversity in supramolecular complexes of  $\text{MCl}_3$  (M = As, Sb, Bi) with constrained thio- and seleno-ether ligands. *Inorg. Chem.* **2010**, *49*, 9036–9048. [[CrossRef](#)]
52. Angilella, V.; Mercier, H.; Belin, C.J. Heteroatomic polyanions of post-transition elements. Synthesis and structure of a salt containing the novel hybrid hepta-arsenic tetraselenate(1-) anion,  $\text{As}_7\text{Se}_4^-$ . *Chem. Soc. Chem. Commun* **1989**, 1654–1655. [[CrossRef](#)]
53. Hill, N.J.; Levason, W.; Patel, R.; Reid, G.; Webster, M. Unusual structural trends in the  $[\text{MCl}_3(\text{[8]aneSe}_2)]$  (M = As, Sb, Bi) adducts. *Dalton Trans.* **2004**, 980–981. [[CrossRef](#)] [[PubMed](#)]
54. Sharma, R.K.; Kedarnath, G.; Jain, V.K.; Wadawale, A.; Nalliath, M.; Pillai, C.G.S.; Vishwanadh, B. 2-Pyridyl selenolates of antimony and bismuth: Synthesis, characterization, structures and their use as single source molecular precursor for the preparation of metal selenidenanostructures and thin films. *Dalton Trans.* **2010**, *39*, 8779–8787. [[CrossRef](#)] [[PubMed](#)]
55. Šimon, P.; Jambor, R.; Růžička, A.; Dostál, L. Oxidative addition of diphenyldichalcogenides  $\text{PhEPh}$  (E = S, Se, Te) to low-valent CN- and NCN-chelated organoantimony and organobismuth compounds. *Organometallics* **2013**, *32*, 239–248. [[CrossRef](#)]
56. Wagner, C.; Merzweiler, K. Neue  $[\{\text{Cp}(\text{CO})_2\text{Mo}\}_2\text{ESbCl}]$ -cluster mit tetraedrischem  $\text{Mo}_2\text{SbE}$ -Gerüst (E = S, Se). *Z. Anorg. Allg. Chem.* **2011**, *637*, 651–654. [[CrossRef](#)]
57. Kimura, M.; Iwata, A.; Itoh, M.; Yamada, K.; Kimura, T.; Sugiura, N.; Ishida, M.; Kato, S. Synthesis, structures, and some reactions of [(thioacyl)thio]- and (acylseleno)antimony and -bismuth derivatives  $(\text{RCSS})_x\text{MR}$  and  $(\text{RCOSe})_x\text{MR}$  with M = Sb, Bi and x = 1–3). *Helv. Chim. Acta* **2006**, *89*, 747–783. [[CrossRef](#)]
58. Martin, T.M.; Wood, P.T.; Kolis, J.W. Synthesis and structure of an  $[\text{Sb}_{12}\text{Se}_{20}]^{4+}$  salt: The largest molecular Zintl ion. *Inorg. Chem.* **1994**, *33*, 1587–1588. [[CrossRef](#)]
59. Breunig, H.J.; Güleç, S.; Krebs, B.; Dartmann, M. Synthese und struktur von  $(\text{MeSe})_3\text{Sb}$ . *Z. Naturforsch. B Chem. Sci.* **1989**, *44*, 1351–1354. [[CrossRef](#)]
60. Sommer, H.; Eichhöfer, A.; Drebov, N.; Ahlrichs, R.; Fenske, D. Preparation, Geometric and electronic structures of  $[\text{Bi}_2\text{Cu}_4(\text{SPh})_8(\text{PPh}_3)_4]$  with a  $\text{Bi}_2$  dumbbell,  $[\text{Bi}_4\text{Ag}_3(\text{SePh})_6\text{Cl}_3(\text{PPh}_3)_3]_2$  and  $[\text{Bi}_4\text{Ag}_3(\text{SePh})_6\text{X}_3(\text{PPh}^i\text{Pr}_2)_3]_2$  (X = Cl, Br) with a  $\text{Bi}_4$  unit. *Eur. J. Inorg. Chem.* **2008**, 5138–5145. [[CrossRef](#)]
61. Shieh, M.; Liu, Y.-H.; Huang, C.-Y.; Chen, S.-W.; Cheng, W.-K.; Chien, L.T. The first naked bismuth–chalcogen metal carbonyl clusters: Extraordinary nucleophilicity of the Bi atom and semiconducting characteristics. *Inorg. Chem.* **2019**, *58*, 6706–6721. [[CrossRef](#)]
62. Calderazzo, F.; Morvillo, A.; Pelizzi, G.; Poli, R.; Ungari, F. Reactivity of molecules containing element–element bonds. 1. Nontransition elements. *Inorg. Chem.* **1988**, *27*, 3730–3733. [[CrossRef](#)]
63. Sommer, H.; Eichhofer, A.; Fenske, D. Bismutchalkogenolate  $\text{Bi}(\text{SC}_6\text{H}_5)_3$ ,  $\text{Bi}(\text{SeC}_6\text{H}_5)_3$  und  $\text{Bi}(\text{S}-4\text{-CH}_3\text{C}_6\text{H}_4)_3$ . *Z. Anorg. Allg. Chem.* **2008**, *634*, 436–440. [[CrossRef](#)]
64. Morikami, A.; Takimiya, K.; Aso, Y.; Otsubo, T. Novel tellurium containing fulvalene-type electron donors, triselenatellurafulvalene (TSTeF) and diselenaditellurafulvalene (DSDTeF); synthesis, conductivities and crystal structures of their TCNQ complexes. *J. Mater. Chem.* **2001**, *11*, 2431–2436. [[CrossRef](#)]

65. Dereu, N.L.M.; Zingaro, R.A.; Meyers, E.A. Bis(4-methoxybenzenetellurenyl)selenide,  $C_{14}H_{14}O_2SeTe_2$ . *Cryst. Struct. Commun.* **1981**, *10*, 1345–1352.
66. Stanford, M.W.; Knight, F.R.; Arachchige, K.S.A.; Camacho, P.S.; Ashbrook, S.E.; Bühl, M.; Slawin, A.M.Z.; Woollins, D.J. Probing interactions through space using spin–spin coupling. *Dalton Trans.* **2014**, *43*, 6548–6560. [[CrossRef](#)] [[PubMed](#)]
67. Hrib, C.G.; Jeske, J.; Jones, P.G.; du Mont, W.-W. Telluroselenophosphonium ions: Their unusual soft–soft interactions with iodotellurate anions. *Dalton Trans.* **2007**, 3483–3485. [[CrossRef](#)] [[PubMed](#)]
68. Klapotke, T.M.; Krumm, B.; Mayer, P.; Piotrowski, H.; Schwab, I.; Vogt, M. Synthesis and structures of triorganotelluronium pseudohalides. *Eur. J. Inorg. Chem.* **2002**, 2701–2709. [[CrossRef](#)]
69. Mathur, P.; Payra, P.; Ghose, S.; Hossain, M.M.; Satyanarayana, C.V.V.; Chicote, F.O.; Chadha, R.K. Synthesis and characterisation of  $[Fe_2M_3(\mu_4-E)(\mu_3-E')(CO)_{17}]$  and  $[Os_3(\mu_3-E)(\mu_3-E')(CO)_9]$  ( $M=Os$  or  $Ru$ ;  $E=S, Se, Te$ ;  $E'=Se, Te$ ). *J. Organomet. Chem.* **2000**, *606*, 176–182. [[CrossRef](#)]
70. Dibrov, S.M.; Ibers, J.A.  $[TeSe_3]^{2-}$  as a tridentate ligand: Syntheses and crystal structures of  $[PPh_4][CpM(\mu_2-Se_2)_3(\mu_3-O)(\mu_3-TeSe_3)]$  ( $M = Zr, Hf$ ). *Comptes Rendus Chim.* **2005**, *8*, 993–997. [[CrossRef](#)]
71. Ogawa, S.; Yoshimura, S.; Nagahora, N.; Kawai, Y.; Mikata, Y.; Sato, R. Novel multi-chalcogen ring systems with three different chalcogen atoms: Synthesis, structure and redox property of five-membered trichalcogenaheterocycles. *Chem. Commun.* **2002**, 1918–1919. [[CrossRef](#)]
72. Åse, K.; Foss, O.; Roti, I. The crystal and molecular structures of trans square-planar complexes of tellurium diselenocyanate with trimethylenethiourea and tetramethylthiourea. *Acta Chem. Scand.* **1971**, *25*, 3808–3820. [[CrossRef](#)]
73. Karjalainen, M.M.; Oilunkaniemi, R.; Laitinen, R.S. Chalcogen–chalcogen interactions in trichalcogenoferrocenophanes. Crystal structure of 2-selena-1,3-ditellura[3]ferrocenophane  $[Fe(C_5H_4Te)_2Se]$ . *Inorg. Chim. Acta* **2012**, *390*, 79–82. [[CrossRef](#)]
74. Karjalainen, M.M.; Sanchez-Perez, C.; Mikko Rautiainen, J.; Oilunkaniemi, R.; Laitinen, R.S. Chalcogen–chalcogen secondary bonding interactions in trichalcogenoferrocenophanes. *CrystEngComm* **2016**, *18*, 4538–4545. [[CrossRef](#)]
75. Nordheider, A.; Hüll, K.; Prentis, J.K.D.; Arachchige, K.S.A.; Slawin, A.M.Z.; Woollins, D.J.; Chivers, T. Main group tellurium heterocycles anchored by a  $P_2^V N_2$  scaffold and their sulfur/selenium analogues. *Inorg. Chem.* **2015**, *54*, 3043–3054. [[CrossRef](#)] [[PubMed](#)]
76. Tiekink, E.R.T. Perplexing coordination behaviour of potentially bridging bipyridyl-type ligands in the coordination chemistry of zinc and cadmium 1,1-dithiolate compounds. *Crystals* **2018**, *8*, 18. [[CrossRef](#)]
77. Tiekink, E.R.T. Supramolecular assembly based on “emerging” intermolecular interactions of particular interest to coordination chemists. *Coord. Chem. Rev.* **2017**, *345*, 209–228. [[CrossRef](#)]
78. Heywood, V.L.; Alford, T.P.J.; Roeleveld, J.J.; Lekanne Deprez, S.J.; Verhoofstad, A.; van der Vlugt, J.I.; Domingos, S.R.; Melanie Schnell, M.; Davis, A.P.; Mooibroek, T.J. Observations of tetrel bonding between  $sp^3$ -carbon and THF. *Chem. Sci.* **2020**, *11*, 5289–5293. [[CrossRef](#)]

